Journal of Materials Chemistry A

RSC Publishing

COMMUNICATION

View Article Online
View Journal | View Issue

High flux CO_2 transporting nanochannel fabricated by the self-assembly of a linear-brush block copolymer†

Cite this: *J. Mater. Chem. A*, 2013, **1**, 8097

Received 19th April 2013
Accepted 3rd June 2013

DOI: 10.1039/c3ta11572k

www.rsc.org/MaterialsA

Baolong Xue,[a] Longcheng Gao,*[a] Heming Jiang,[a] Zhi Geng,[a] Song Guan,[a] Yao Wang,[a] Zhiwen Liu[b] and Lei Jiang*[ac]

Linear-brush poly(styrene)-*b*-poly[oligo(ethylene glycol) methyl ether methacrylate] (PS-*b*-POEGMA) block copolymer incorporating a UV-crosslinkable coumarin group in a PS block, self-assembled into a cylindrical structure with POEGMA cylinders perpendicular to the film surface, which exhibit excellent CO_2 separation properties. The block copolymer was successfully synthesized by a combination of atom transfer radical polymerization (ATRP) and click chemistry. The molecular characterization of the diblock copolymer was performed with ^1H nuclear magnetic resonance (NMR) and gel permeation chromatography (GPC). The cylindrical phase structure was confirmed by small angle X-ray scattering (SAXS), transmission electron microscopy (TEM) and atomic force microscopy (AFM). The POEGMA amorphous phase was confirmed by differential scanning calorimeter (DSC). Gas permeation properties of CO_2, N_2 and He were determined around room temperature. Compared to the linear BCP, the total gas selectivity and especially CO_2 permeation flux increased dramatically. The functional block units and self-assembled microphase structures synergetically played key roles in the high performance of the membrane.

CO_2 emission has been assigned to be a major factor in global warming. CO_2 separation by membranes has attracted great interests due to its energy efficiency.[1] Two factors determine the performance of a membrane gas separation system: permeability and selectivity. There exists an upper bound trade-off curve, relating permeability and selectivity.[2] The driving force for gas flow is the pressure difference across the membrane. The driving force for the flow of the highly selective gas will be lower than that of the nonselective gas without using a sweep gas, which is normally performed in industry. For a membrane with a high intrinsic selectivity and low permeability, compressing the feed stream or drawing a vacuum on the permeate side to maintain the driving force, requires extra energy and process equipment. Therefore, for industrial gas separations, membranes with high permeability and moderate selectivity are in demand, especially in multistep membrane separation.[3]

Among the CO_2 separation technologies, block copolymer (BCP) membrane separation is a promising technology. BCPs, taking advantage of the ordered nanostructures throughout the membrane, provide CO_2 transporting nanochannels and exhibit outstanding separation properties. Furthermore, BCPs are easy to synthesise for membrane preparation. Polyethylene oxide (PEO) based polymers are preferred to be the CO_2-philic functional group, due to the high affinity between ether oxygen (EO) linkages and CO_2.[2b,4] Di-, tri-BCP and segmented BCP,[5] containing PEO has been synthesized. The CO_2 separation performance can be tailored by controlling the PEO molecular weight and volume fraction.[5a,c,6] High PEO content results in high CO_2 separation properties.[7] However, PEO with high molecular weight has a negative effect on the gas permeability because of its strong tendency to crystallize. Crystal PEO limits the amount of the permeable amorphous phase, and furthermore reduces the chain mobility. Methods, such as blending liquid PEO with compatible solid polymers, crosslinking PEO to form networks,[4b] incorporating PPO randomly,[8] and so on, have been carried out to depress crystallization. In previous work, we have researched BCP with linear PEO ($M_n = 2000$), which self-assembled into a cylindrical structure, with PEO cylinders oriented perpendicular to the surface.[9] Due to the fact that PEO is semi-crystal the CO_2 diffusivity and selectivity was low at room temperature.

Here, for the first time, we introduce brush-type PEO into BCP, from oligo(ethylene glycol) (OEG) monomers, to form soft CO_2 transporting nanochannels with well defined features. Brush-type or bottle brush-like polymers composed of a linear backbone and a high grafting density of OEG side chains is

[a]*Key Laboratory of Bio-inspired Smart Interfacial Science and Technology of Ministry of Education, School of Chemistry and Environment, Beihang University, Beijing, 100191, P.R. China. E-mail: lcgao@buaa.edu.cn; jianglei@iccas.ac.cn*

[b]*Agilent Technologies, No.3, Wang Jing Bei Lu, Chao Yang District, Beijing, 100102, P. R. China*

[c]*Beijing National Laboratory for Molecular Sciences (BNLMS), Key Laboratory of Organic Solids, Institute of Chemistry, Chinese Academy of Sciences, Beijing, 100190, P. R. China*

† Electronic supplementary information (ESI) available. See DOI: 10.1039/c3ta11572k

among the most intriguing macromolecular structures. Brush-like polymers with OEG short chains have extremely low glass transition temperatures. The higher content of methyl ether end group increases the free volume and hinders the EO crystallization. Therefore, the CO_2 permeability and selectivity is expected to be enhanced.[10]

The design structure and synthetic procedure is shown in Scheme 1. A PS block with random UV-crosslinkable coumarin units was synthesized by ATRP, for physical and mechanical consideration, as well being used for free-standing film fabrication. The soft EO block was then incorporated by a combination of click chemistry and ATRP in a one-pot process, obtaining well controlled BCP.

The linear-brush BCP was also synthesized by a combination of click chemistry and ATRP in a one-pot process. Such a combination is a powerful macromolecular engineering tool, and provides well-defined BCP structures.[11] Sequential ATRP was not applied because of low initiation efficiency of the macroinitiator in the system.

Fig. S1† shows the GPC curves of the original PS macroinitiator (a) and BCP (b). Comparison to the starting PS macroinitiator ($M_n = 21.0$ k, PDI = 1.17), a visible unimodal shift to higher molecular weight is seen. The polydispersity is relatively low ($M_n = 28.9$ k, PDI = 1.17). ^{1}H NMR measurements were employed to confirm the structure and to calculate the composition of the copolymers. The BCP ^{1}H NMR spectrum is shown in Fig. S2.† The characteristic peaks of the PS block are located in the range of δ from 6.3 to 7.2 ppm. The characteristic peak at $\delta = 2.4$ ppm was assigned to the methylene protons in the coumarin group, the peak around $\delta = 5.0$ ppm corresponds to the benzyl protons, and the peak around $\delta = 6.2$ ppm corresponds to the proton of double bond (C=CH) adjacent to the carbonyl group. The weight percent of the POEGMA brush is calculated around 39.2%.

An FT-IR experiment was also applied to monitor the synthetic procedure. Fig. S3† shows the FT-IR spectra of PS–Br, PS–N_3, and PS-*b*-POEGMA. Comparison of the spectra in Fig. 3a and b, shows the appearance of a peak at 2095 cm^{-1}, corresponding to the –N_3 group. This peak totally disappeared in Fig. 3c, indicating a successful click reaction, confirmed by the appearance of the characteristic absorption bands at 1730 cm^{-1} (C=O stretching vibration) and 1111 cm^{-1} (C–O–C stretching vibration), which confirms the presence of POEGMA.

DSC is employed to confirm the thermal transitions of BCP. The DSC curve for BCP is shown in Fig. 1a. Two glass transitions are clearly detected, indicating a degree of microphase separation between the PS and POEGMA blocks. The signal at around −64 °C is identified as T_g of the POEGMA block and the other at around 84 °C as T_g of the PS block. The DSC analysis shows that the BCP exhibits microphase separation. It is worthy of note that, the linear PEO with high molecular weight is crystallized, as mentioned above. However, the brush-like POEGMA is amorphous, determined from the absence of any melting point on the DSC curve. Also, no scattering peaks can be seen from wide angle X-ray scattering characterization of POEGMA and BCP (see Fig. S4 and S5†). Indeed, the POEGMA homopolymer is a kind of glue at room temperature. The self-assembled structure of the BCP is detected by SAXS. Fig. 1b shows the SAXS curve at room temperature. It can be found that the primary peak centered around a scattering wave vector q value corresponding of ~28 nm. In addition, higher order reflections are visible at angular positions of $\sqrt{3}$, $\sqrt{4}$ and $\sqrt{7}$ of the first-order maximum, indicative of the hexagonal phase.

To confirm the structure of BCP, AFM and TEM experiments were carried out. Fig. 2a and b show the AFM topography and phase images of the BCP film. An array of nanoscopic dots is seen on the surface of the BCP film. Considering the weight fraction of the BCP, the dark dots in the topography and phase image are attributed to the POEGMA phase within the bright PS matrix. The

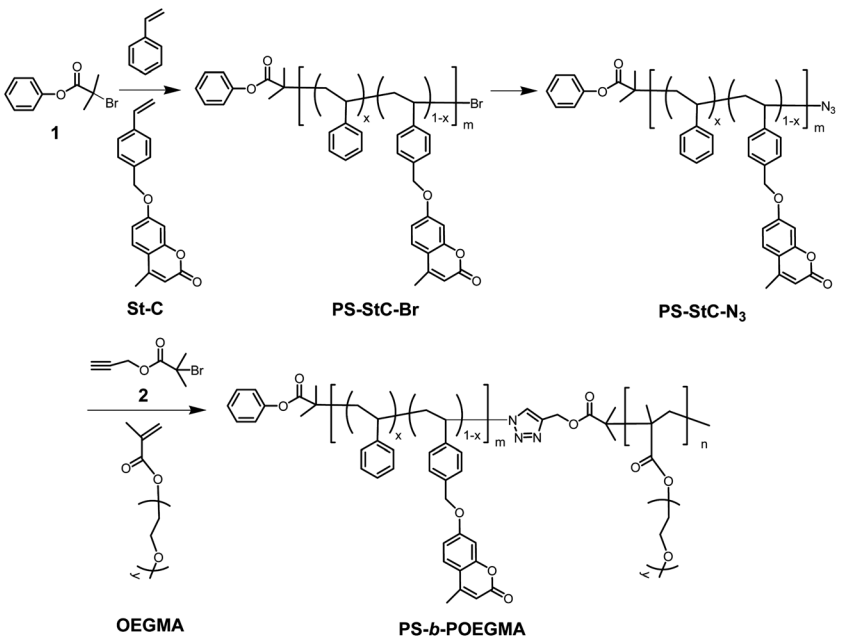

Scheme 1 The synthetic procedure for UV-crosslinkable BCP containing POEGMA brushes.

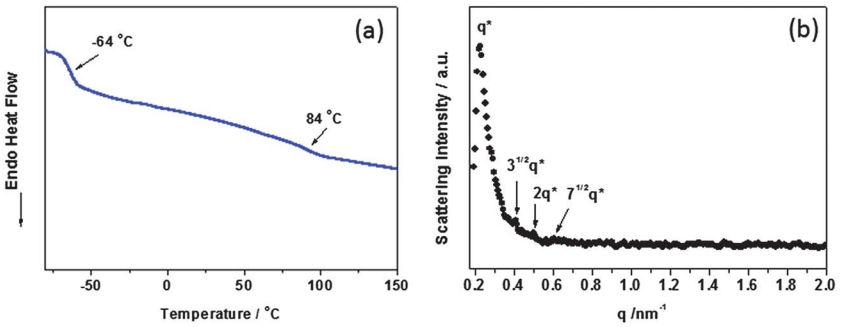

Fig. 1 (a) The DSC curve of BCP, showing two distinct T_g at around −64 °C and 84 °C. (b) SAXS of the BCP. The higher order scattering vectors indicate hexagonal phase structure.

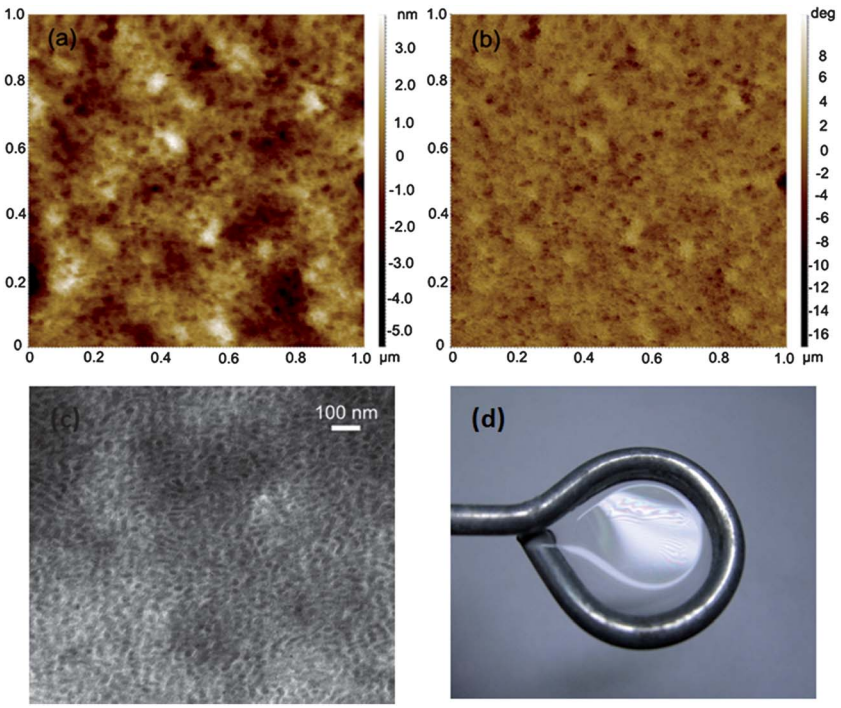

Fig. 2 AFM height (a) and phase (b) images of the BCP film. (c) TEM image of the block copolymer film (POEGMA was selectively stained by RuO_4), indicating perpendicular cylinders to the surface. (d) A digital photograph of the free-standing film detached from the silicon wafer by dissolving the CA sacrifice layer.

cylindrical nanodomains of POEGMA are oriented normal to the substrate. The AFM results coincide with the SAXS result. One drop of BCP solution (4%) in toluene was put onto a TEM grid, and then absorbed immediately by filter paper. The grid was placed in benzene vapor for 2 h at room temperature, dried in a N_2 atmosphere over night, and then under vacuum elevating the temperature gradually from ambient temperate to 80 °C. The TEM micrograph shown in Fig. 2c gives a clear view of the dot structures. Stained POEGMA (black parts) disperse in the PS matrix. Although hexagonal symmetry is absent, which may be attributed to the substrate effect, the basic requirement of perpendicular POEGMA cylinders throughout the film is realized.

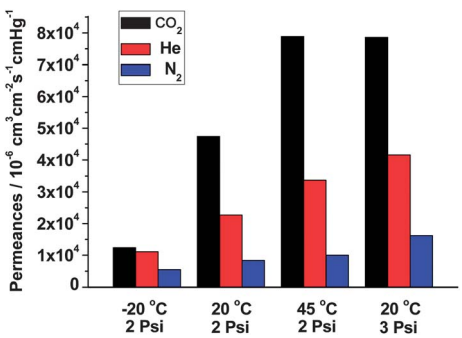

Fig. 3 Gas permeances for CO_2 (black), He (red), and N_2 (blue) at different temperature and upstream pressure, indicating higher CO_2 diffusivity.

A free standing film is obtained by UV exposure of the BCP film. The coumarin moieties located randomly in the PS domains react through the [2 + 2] cyclization of the double bond. According to the previous studies,[9] the UV-crosslinking step was carried on within 5 min. The UV-crosslinking film can be detached from the substrate by dissolving the sacrifice layer (Fig. 2d). Films with arbitrary size can be obtained depending on the substrates.

Gases permeation measurements are carried out with a home-built permeation apparatus described previously. The tested BCP film has an average thickness of 3.6 μm. The results are listed in Fig. 3. At 20 °C, with upstream pressure of 3 psi, the membrane has a permeance of 78 600 × 10^{-6} cm^3 cm^{-2} s^{-1} $cmHg^{-1}$, one order higher than that of BCP with linear PEO under the same condition, which is 2160 × 10^{-6} cm^3 cm^{-2} s^{-1} $cmHg^{-1}$. Furthermore, the CO_2 selectivity over N_2 and He is also higher than previously reported.[9] The key point is that the PEO in the nanochannels is totally amorphous. The performance is also much higher than that of poly(1-trimethylsilyl-1-propyne) (PTMSP), which has one of the highest CO_2 permeabilities,[12] and surpassing the Robeson's upper bound.[2] At 20 °C with a lower upstream pressure of 2 psi, although all the gases permeances reduce, the CO_2 selectivity slightly increases (see Table S1†). Increasing to 45 °C, the CO_2 permeances increase to the higher value of 78 900 × 10^{-6} cm^3 cm^{-2} s^{-1} $cmHg^{-1}$, and the CO_2 selectivity also increases.

The extremely high gas permeability of the BCP film is attributed to the molecular topological structure and self assembled nanostructures. As discussed above, the linear-brush BCP forms CO_2 transporting nanochannels throughout the membrane. Compared to the linear BCP, the nanochannels are composed of amorphous EO units, with low T_g, instead of semi-crystal PEO. The amorphous PEO nanochannels have high CO_2 affinity and a large excess free volume. Furthermore, the nanochannels throughout the membrane benefit the CO_2 diffusivity. Thus, the gas permeance is greatly enhanced.

In conclusion, UV-crosslinkable linear-brush PS-*b*-POEGMA were successfully synthesized by combination ATRP and click chemistry with the coumarin group randomly located along the PS chain. The BCP self-assembled into a cylindrical structure with POEGMA cylinders perpendicular to the film surface. Taking advantages of both the POEGMA chain morphology and self assembled nanostructures, the film exhibited extremely high CO_2 flux with moderate selectivity over N_2 and He under low upstream pressure. These results provide potential application in multistep CO_2 membrane separation. Further exploitation of this feature is still under investigation.

Acknowledgements

The authors are grateful for financial support from the National Natural Science Foundation of China (21204002), Specialized Research Fund for the Doctoral Program of Higher Education (20111102120050), Program for New Century Excellent Talents in University (2010) and the Fundamental Research Funds for the Central Universities.

References

1 (*a*) P. Bernardo, E. Drioli and G. Golemme, *Ind. Eng. Chem. Res.*, 2009, **48**, 4638–4663; (*b*) N. Du, H. B. Park, M. M. Dal-Cina and M. D. Guiver, *Energy Environ. Sci.*, 2012, **5**, 7306–7322; (*c*) D. L. Gin and R. D. Noble, *Science*, 2011, **332**, 674–676.

2 (*a*) L. M. Robeson, *J. Membr. Sci.*, 1991, **62**, 165–185; (*b*) H. Lin and B. D. Freeman, *J. Mol. Struct.*, 2005, **739**, 57–74.

3 (*a*) R. W. Baker, *Membrane technology and applications*, John Wiley &Sons, Ltd, 2nd edn, 2004; (*b*) P. Shao, M. M. Dal-Cin, M. D. Guiver and A. Kumar, *J. Membr. Sci.*, 2013, **427**, 451–459; (*c*) N. Du, H. B. Park, G. P. Robertson, M. M. Dal-Cin, T. Visser, L. Scoles and M. D. Guiver, *Nat. Mater.*, 2011, **10**, 372–375; (*d*) N. Du, M. M. Dal-Cin, G. P. Robertson and M. D. Guiver, *Macromolecules*, 2012, **45**, 5134–5139.

4 (*a*) Y. Hirayama, Y. Kase, N. Tanihara, Y. Sumiyama, Y. Kusuki and K. Haraya, *J. Membr. Sci.*, 1999, **160**, 87–99; (*b*) H. Lin, E. Wagner, B. D. Freeman, L. G. Toy and R. P. Gupta, *Science*, 2006, **311**, 639–642; (*c*) H. Lin and B. D. Freeman, *J. Membr. Sci.*, 2004, **239**, 105–117.

5 (*a*) S. J. Metz, M. H. V. Mulder and M. Wessling, *Macromolecules*, 2004, **37**, 4590–4597; (*b*) A. Car, C. Stropnik, W. Yave and K. V. Peinemann, *J. Membr. Sci.*, 2008, **307**, 88–95; (*c*) A. Car, C. Stropnik, W. Yave and K. V. Peinemann, *Adv. Funct. Mater.*, 2008, **18**, 2815–2823; (*d*) D. Husken, T. Visser, M. Wessling and R. J. Gaymans, *J. Membr. Sci.*, 2010, **346**, 194–201; (*e*) V. I. Bondar, B. D. Freeman and I. Pinnau, *J. Polym. Sci., Part B: Polym. Phys.*, 2000, **38**, 2051–2062; (*f*) S. R. Reijerkerk, A. Arun, R. J. Gaymans, K. Nijmeijer and M. Wessling, *J. Mater. Sci.*, 2010, **359**, 54–63; (*g*) H. Y. Zhao, Y. M. Cao, X. L. Ding, M. Q. Zhou and Q. Yuan, *J. Mater. Sci.*, 2008, **323**, 176–184.

6 (*a*) A. A. Deschamps, D. W. Grijpma and J. Feijen, *Polymer*, 2001, **42**, 9335–9345; (*b*) M. E. Arnold, K. Nagai, B. D. Freeman, R. J. Spontak, D. E. Betts, J. M. DeSimone and I. Pinau, *Macromolecules*, 2001, **34**, 5611–5619; (*c*) N. P. Patel, A. C. Miller and J. Spontak, *Adv. Funct. Mater.*, 2004, **14**, 699–707.

7 (*a*) W. Yave, A. Car, S. S. Funari, S. P. Nunes and K.-V. Peinemann, *Macromolecules*, 2010, **43**, 326–333; (*b*) K. Okamoto, M. Fujii, S. Okamyo, H. Suzuki, K. Tanaka and H. Kita, *Macromolecules*, 1995, **28**, 6950–6956; (*c*) C. Damain, E. Espuche, M. Escoubes, S. Cuney and J. P. Pascault, *J. Appl. Polym. Sci.*, 1997, **65**, 2579–2587.

8 A. C. IJzer, A. Arun, S. R. Reijerkerk, K. Nijmeijer, M. Wessling and R. J. Gaymans, *J. Appl. Polym. Sci.*, 2010, **117**, 1394–1404.

9 B. L. Xue, X. W. Li, L. C. Gao, M. Gao, Y. Wang and L. Jiang, *J. Mater. Chem.*, 2012, **22**, 10918–10923.

10 S. R. Reijerkerk, A. C. IJzer, K. Nijmeijer, A. Arun, R. J. Gaymans and M. Wessling, *ACS Appl. Mater. Interfaces*, 2010, **2**, 551–560.

11 (*a*) V. V. Rostovtsev, L. G. Green, V. V. Fokin and K. B. Sharpless, *Angew. Chem., Int. Ed.*, 2002, **41**, 2596–2599; (*b*) A. J. de Graaf, E. Mastrobattista, C. F. van Nostrum, D. T. S. Rijkers, W. E. Hennink and T. Vermonden, *Chem. Commun.*, 2011, **47**, 6972–6974; (*c*) L. Mespouille, M. Vachaudez, F. Suriano, P. Gerbaux, O. Coulembier, P. Degée, R. Flammang and P. Dubois, *Macromol. Rapid Commun.*, 2007, **28**, 2151–2158.

12 Y. Hu, M. Shiotsuki, F. Sanda and T. Masuda, *Chem. Commun.*, 2007, 4269–4270.

